IEEE Photonics Journal
An IEEE Photonics Society Publication

Spatial-Dependent Hamiltonian Formulation of Cross-Mode Modulation

Volume 12, Number 1, February 2020

Haofan Yang
Zhongfei Xiong
Hanwen Hu
Yuntian Chen
Xinliang Zhang
Jing Xu

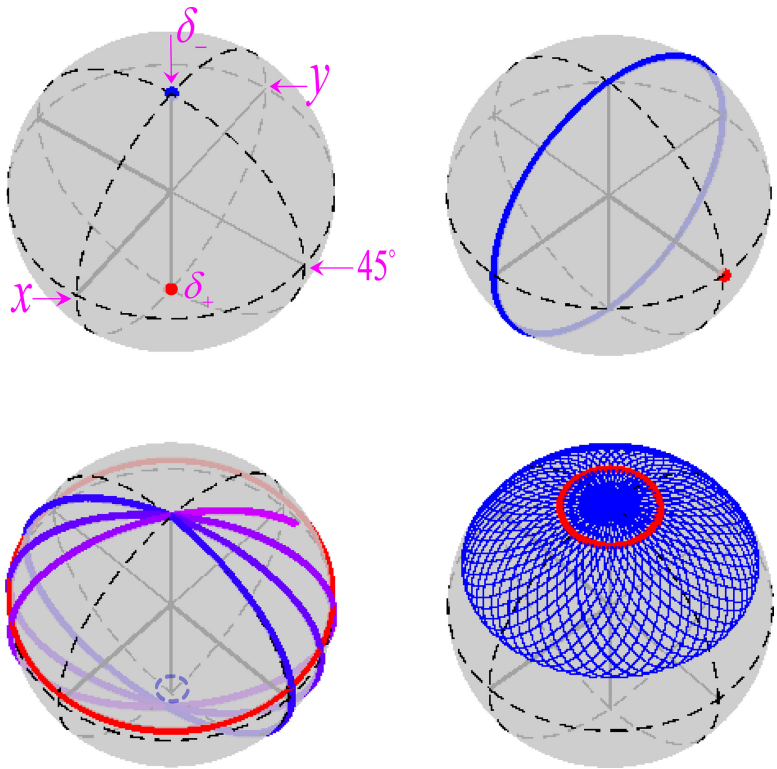

DOI: 10.1109/JPHOT.2019.2960091

Spatial-Dependent Hamiltonian Formulation of Cross-Mode Modulation

Haofan Yang,[1] Zhongfei Xiong,[1] Hanwen Hu,[1] Yuntian Chen,[1,2] Xinliang Zhang ,[1,2] and Jing Xu [1,2]

[1]School of Optical and Electronic Information, Huazhong University of Science and Technology, Wuhan 430074, China
[2]Wuhan National Laboratory for Optoelectronics, Huazhong University of Science and Technology, Wuhan 430074, China

DOI:10.1109/JPHOT.2019.2960091

Manuscript received September 16, 2019; revised December 6, 2019; accepted December 12, 2019. Date of publication December 16, 2019; date of current version January 7, 2020. This work was supported in part by National Natural Science Foundation of China (NSFC) under Grants 61735006 and 61775063, in part by National Key Research and Development Program of China under Grant 2017YFA0305200, and in part by the Fundamental Research Funds for the Central Universities, HUST under Grant 2018KFYYXJJ055. Corresponding author: Jing Xu. (e-mail: jing_xu@hust.edu.cn).

Abstract: In the absence of random mode mixing (RMM), linearization of the cross-mode modulation (XMM) under pump-probe configuration is in general complicated because the evolution of the pump light depends on the local mode decomposition of itself. In this work, general derivation of the Hamiltonian of the XMM system without RMM is carried out and discussed under two interesting scenarios where the pump evolution can be effectively linearized, leading to spatial dependent Hamiltonian of the probe light. Representative evolutions of pump and probe light over transmission are investigated with the assistance of Poincaré sphere based on the Hamiltonian approach. Our results are benchmarked against the results given by precession equations examined by Lin and Agrawal and numerical simulations using nonlinear coupled mode equations (CMEs). By highlighting the eigenstates as well as eigenvalues of the system, our approach provides an intuitive yet powerful approach to understand the XMM nonlinear problems and to dynamically manipulate the spatial profiles of the probe light.

Index Terms: Fiber non-linear optics, Kerr effect.

1. Introduction

Cross-Mode modulation (XMM) describes the rotation of the mode profile of a weak probe light induced by a strong co-propagating pump light in multimode nonlinear optical waveguides [1]–[3]. In case of single mode waveguides, cross-phase modulation between the probe and pump light that are not co-polarized, e.g. nonlinear polarization rotation, can be understood as a special case of XMM and has been widely analyzed [4], [5]. The XMM in multimode optical waveguides induced by third order non-linearity has received broad interests recently due to the rapid progresses in spatial division multiplexing technologies developed for optical fiber communications [6]. Multimode nonlinear Schrödinger equation (MNLSE) [7] is widely used to describe the dispersion and nonlinear effects in multimode optical waveguides, including XMM effect, which is routinely modelled numerically due to the coexistence of dispersion and nonlinearity. Although MNLSE can be greatly simplified in the case of continuous-wave injection, the nonlinear nature of the

coupled differential equations hinders a simpler picture of the underlying physics as those would be found for linear systems. Fortunately, in a commonly applied pump-probe configuration where the evolution of a weak probe light is determined by a strong pump light, the nonlinear problem of XMM can be effectively linearized, rendering a completely different yet powerful treatment, i.e., the Hamiltonian approach [8]. Notably, the Hamiltonian approach is a standard approach in quantum mechanics for studying linear systems. The terminology Hamiltonian itself refers to the energy of the system, and thus governs the evolution of the system. When propagating along multimode fibers, mode couplings can occur randomly due to stress, bending, or technological irregularities of the fibers. Such random mode mixing (RMM) may easily happen between modes with degenerate propagation constants. In an initial attempt of Hamiltonian approach in analyzing the XMM in degenerate mode group with random mode mixing (RMM), which greatly simplifies the coupling equations [1], we reveal the prediction as well as manipulation of the probe mode distribution with a clear picture of nonlinear birefringence [9], where the energy operator, i.e., the Hamiltonian of the system, indicates the allowed nonlinear propagation constants of probe light, derived by calculating the corresponding eigenvectors and eigenvalues. Notably, our previous work is typically for optical fibers, where RMM plays a relevant role. However, the restriction of RMM as well as degenerate mode group limits the applications in other scenario such as integrated photonic circuit where the required interaction length can be made very short due to strong mode confinement [10]. In addition, XMM effect between non-degenerate mode group are also topics of active research interests [2]. Therefore, Hamiltonian approach of linearizing the complex nonlinear dynamics is also very appearing. In this work, we propose a generalized Hamiltonian approach that is capable of analyzing the XMM without RMM. Two important scenarios in terms of differential propagation constant ($\Delta\beta$) between interacting modes are discussed. It is shown that the Hamiltonian of the probe light turns out to be spatially dependent, leading to fundamentally different properties from our previous analysis where the Hamiltonian is independent of propagation coordinates [9].

2. Hamiltonian Framework of XMM Without RMM

Instead of using generalized Manakov equation that deals with a modal group containing N degenerate modes with RMM [1], [9], we start from MNLSE [7], [11] for interaction between modes and consider the case without loss and dispersion

$$\frac{\partial \vec{E}}{\partial z} = i\gamma \sum_{jhkm} C_{jhkm} E_h^* E_k E_m \hat{e}_j, \tag{1}$$

where $\vec{E}(z,t)$ represents the optical field envelope of $2N$ spatial modes including polarization. With the set of complex unit vectors $\hat{e}_j$, $j = 1, \ldots, 2N$, to represent an orthogonal mode basis, the total electrical field can be written as $\vec{E} = \sum_j E_j \hat{e}_j$. The dimensionless constants C_{jhkm} account for the spatial mode overlap integrals [11], and γ is the nonlinear parameter. The impact of transmission loss can be taken into consideration by defining an effective length, i.e., $L_{eff} = (1 - e^{-\alpha z})/\alpha$, where α is the loss coefficient [9]. By replacing the transmission length z with the effective length, loss can be included in the nonlinear coupled mode equations as well as subsequent derived Hamiltonians. Without loss of generality, dispersion terms are dropped to highlight the linear property behind the nonlinear problem [1], [12], [13], as valid in case of continuous waves (CWs) or even pulses whenever the fiber length is much shorter than the dispersion length as well as walk off length [12]. We consider the pump-probe configuration in a two modes coupling system, where the two modes may be different from spatial distribution, polarization, or both. The total optical field at the input of the nonlinear waveguide can be written as $\vec{E} = \vec{a} + \vec{b}$, where $\vec{a} = a_1 e^{i\beta_1 z}\hat{e}_1 + a_2 e^{i\beta_2 z}\hat{e}_2$ and $\vec{b} = b_1 e^{j\beta_1 z}\hat{e}_3 + b_2 e^{j\beta_2 z}\hat{e}_4$ with modal label $j = 1, 2$ corresponding to the two modes at λ_a (probe light) while $j = 3, 4$ to the same modes but at wavelength λ_b (pump light). β_1 and β_2 represent the linear propagation constants of the two modes without pump-induced nonlinearity and $\Delta\beta = \beta_1 - \beta_2$. The

coupled mode equations can be cast as:

$$\frac{\partial}{\partial z}\begin{pmatrix} a_1 & a_2 \end{pmatrix}^T = iH_a \begin{pmatrix} a_1 & a_2 \end{pmatrix}^T, \tag{2a}$$

$$\frac{\partial}{\partial z}\begin{pmatrix} b_1 & b_2 \end{pmatrix}^T = iH_b \begin{pmatrix} b_1 & b_2 \end{pmatrix}^T, \tag{2b}$$

where $H_a = (H_{a_{11}}, H_{a_{12}}; H_{a_{21}}, H_{a_{22}})$, $H_b = (H_{b_{11}}, H_{b_{12}}; H_{b_{21}}, H_{b_{22}})$,

$$\begin{aligned}
H_{a_{11}} &= \gamma \left\{ (C_{1313} + C_{1331}) |b_1|^2 + (C_{1414} + C_{1441}) |b_2|^2 \right. \\
&\quad \left. + (C_{1314} + C_{1341}) e^{-i\Delta\beta z} b_1^* b_2 + (C_{1413} + C_{1431}) e^{i\Delta\beta z} b_1 b_2^* \right\}, \\
H_{a_{12}} &= \gamma \left\{ (C_{1323} + C_{1332}) e^{-i\Delta\beta z} |b_1|^2 + (C_{1424} + C_{1442}) e^{-i\Delta\beta z} |b_2|^2 \right. \\
&\quad \left. + (C_{1423} + C_{1432}) b_1 b_2^* + (C_{1342} + C_{1324}) e^{-2i\Delta\beta z} b_1^* b_2 \right\}, \\
H_{a_{21}} &= \gamma \left\{ (C_{2313} + C_{2331}) e^{i\Delta\beta z} |b_1|^2 + (C_{2414} + C_{2441}) e^{i\Delta\beta z} |b_2|^2 \right. \\
&\quad \left. + (C_{2314} + C_{2341}) b_1^* b_2 + (C_{2431} + C_{2413}) e^{2i\Delta\beta z} b_1 b_2^* \right\}, \\
H_{a_{22}} &= \gamma \left\{ (C_{2424} + C_{2442}) |b_2|^2 + (C_{2323} + C_{2332}) |b_1|^2 \right. \\
&\quad \left. + (C_{2324} + C_{2342}) e^{-i\Delta\beta z} b_1^* b_2 + (C_{2432} + C_{2423}) e^{i\Delta\beta z} b_1 b_2^* \right\},
\end{aligned}$$

and

$$\begin{aligned}
H_{b_{11}} &= \gamma \left\{ C_{3333} |b_1|^2 + (C_{3434} + C_{3443}) |b_2|^2 + C_{3433} e^{i\Delta\beta z} b_1 b_2^* \right\}, \\
H_{b_{12}} &= \gamma e^{-i\Delta\beta z} \left\{ C_{3344} e^{-i\Delta\beta z} b_1^* b_2 + (C_{3334} + C_{3343}) |b_1|^2 + C_{3444} |b_2|^2 \right\}, \\
H_{b_{21}} &= \gamma e^{i\Delta\beta z} \left\{ C_{4433} e^{i\Delta\beta z} b_1 b_2^* + (C_{4443} + C_{4434}) |b_2|^2 + C_{4333} |b_1|^2 \right\}, \\
H_{b_{22}} &= \gamma \left\{ C_{4444} |b_2|^2 + (C_{4343} + C_{4334}) |b_1|^2 + C_{4344} e^{-i\Delta\beta z} b_1^* b_2 \right\}.
\end{aligned}$$

Eq. (2a) gives the general Hamiltonian formalism for the XMM problem, which can be used to solve the evolution of the probe light. It is clear that the components of probe Hamiltonian, H_a, depends on b_1 and b_2 but is independent of a_1 and a_2, which is exactly the feature of pump-probe configuration.

3. Spatial Dependent Hamiltonian in Two Special Scenarios

According to Eq. (2), pump light evolves nonlinearly since the evolution of b_1 and b_2 depends on their local values, as indicated by H_b. It is thus more useful to derive an expression of H_a which is only determined by the initial conditions of the pump light as well as waveguide properties. To do this, we will be focused on two specific scenarios in the rest of the paper, where explicit analytical expression of H_a can be derived. That is, the beat length $L_B = 2\pi/|\Delta\beta|$ is either much shorter (scenario I) or sufficient longer (scenario II) than the nonlinear interaction length $L_{NL} = 1/\gamma P_p$, where P_p is the total pump power. It will be shown later that H_b can be effectively linearized/diagonalied in these two cases.

3.1 Scenario I: XMM Between Degenerate Modes

First we consider scenario I, i.e., $L_B \gg L_{NL}$. Physically, this means that $\Delta\beta$ between two interacting modes is sufficiently small, corresponding to the case of mode degenerancy. To be concrete, we investigate the XMM coupling between two orthrogoally polarized fundamental modes of an optical fiber without birefringence and $\Delta\beta$ is approximated as zero. This is actually the case of

polarization evolutions under cross-phase modulation in isotropic single mode waveguides. By neglecting the frequency dependence of the transverse mode profile, the nonzero coefficients of C_{jhkm} appear in Eq. (2) are $C_{1313} = C_{1331} = C_{2424} = C_{2442} = C_{3333} = C_{4444} = 1$, $C_{1441} = C_{1423} = C_{2314} = C_{2332} = C_{3443} = C_{4334} = 2/3$, $C_{1342} = C_{1324} = C_{2431} = C_{2413} = C_{3344} = C_{4433} = 1/3$ [14]. Defining $a_\pm = (a_1 \pm ia_2)/\sqrt{2}$, $b_\pm = (b_1 \pm ib_2)/\sqrt{2}$, where $+$ and $-$ corresponds to the right- and left-handed circularly polarized states (δ_+ and δ_-), Eq. (2) becomes

$$\frac{\partial |a\rangle}{\partial z} = iH'_a |a\rangle , \tag{3a}$$

$$\frac{\partial |b\rangle}{\partial z} = iH'_b |b\rangle , \tag{3b}$$

where $|a\rangle = (a_+ \quad a_-)^T$, $|b\rangle = (b_+ \quad b_-)^T$, and

$$H'_a = \frac{4}{3}\begin{pmatrix} |b_+|^2 + |b_-|^2 & b_+ b_-^* \\ b_+^* b_- & |b_-|^2 + |b_+|^2 \end{pmatrix}, H'_b = \frac{2}{3}\begin{pmatrix} |b_+|^2 + 2|b_-|^2 & 0 \\ 0 & |b_-|^2 + 2|b_+|^2 \end{pmatrix}.$$

Note that Eq. (3b) is nonlinear on the first sight because H'_b is dependent on $|b\rangle$. However, H'_b is a diagonal matrix which means there is no energy coupling between δ_+ and δ_-, indicating that δ_+ and δ_- are the eigenmodes of the pump light. This gives an intuitive explanation of selection of circularly polarized mode basis instead of LP mode basis in [12]. Therefore, the modulus of δ_+ and δ_- become independent of z. By defining the initial condition of $|b\rangle$ at $z = 0$ as $\sqrt{P_p}(p \quad q)^T$, where p and q are the normalized complex amplitudes that satisfy $|p|^2 + |q|^2 = 1$, the Hamiltonian of the pump can be written as

$$H'_b = \frac{2}{3}\gamma P_p \begin{pmatrix} |q|^2 + 1 & 0 \\ 0 & |p|^2 + 1 \end{pmatrix}, \tag{4}$$

and the eigenvectors and eigenvalues are found to be

$$\vec{v} = \{\{1, 0\}, \{0, 1\}\}, \quad \zeta_b = \{\zeta_{b_1}, \zeta_{b_2}\} = \frac{2}{3}\gamma P_p\{|q|^2 + 1, |p|^2 + 1\}. \tag{5}$$

The Hamiltonian of the probe light determined by the pump light becomes

$$H'_a = \frac{4}{3}\gamma P_p \begin{pmatrix} 1 & pq^* e^{j\Delta\zeta_b z} \\ p^* q e^{-j\Delta\zeta_b z} & 1 \end{pmatrix}, \tag{6}$$

where $\Delta\zeta_b = \zeta_{b_1} - \zeta_{b_2}$. So far an explicit expression of the probe Hamiltonian is written out, which is in general spatially dependent. The evolution of the probe light over transmission can be derived numerically by sequentially calculating the linear superposition of eigenstates with nonlinear phase shifts [9] over over small steps [15]. However, in case of $pq = 0$ or $|p| = |q|$ ($\Delta\zeta_b = 0$), the spatial dependence can be eliminated, according to Eq. (6). In this case, the evolution of probe light can be analytically expressed since the eigenstates are z invariant [9]. In the following, the evolution of the state of polarization (SOP) of the pump and probe light are elaborated and visualized on Poincaré sphere using Stokes vectors, as shown in Fig. 1. Pump is represented by red dots/lines and probe by blue/purple dots/lines. The stokes vectors of the pump and probe are defined as $\vec{m} = \langle b|\vec{\sigma}|b\rangle$ and $\vec{n} = \langle a|\vec{\sigma}|a\rangle$, respectively. The vector $\vec{\sigma}$ is defined using the unit vectors $\hat{k}_j$ as $\vec{\sigma} = \sigma_1\hat{k}_1 + \sigma_2\hat{k}_2 + \sigma_3\hat{k}_3$ and $\sigma_j (j = 1, 2, 3)$ are the three Pauli matrices [16]. In all cases, the initial SOP of the probe light is fixed at δ_-. The evolution pattern of the probe and pump light under different initial pump SOP are explained as follows. Figure 1(a) shows the case of $pq = 0$, where the initial SOP of the pump could be either at δ_+ or δ_- and δ_+ is used in this case. The corresponding eigenvectors and eigenvalues of the probe light are

$$\vec{u} = \{\{1, 0\}, \{0, 1\}\}, \quad \zeta_a = \frac{4}{3}\gamma P_p\{1, 1\}. \tag{7}$$

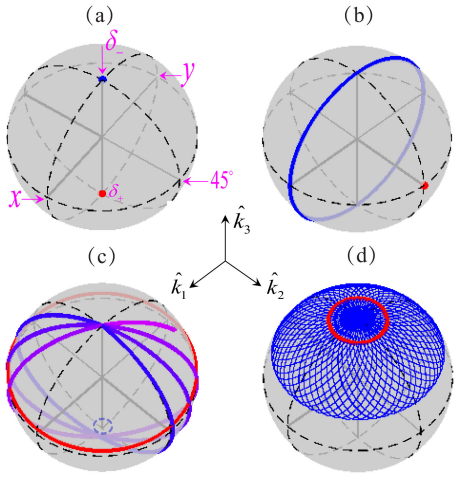

Fig. 1. Evolution of the SOP of pump light (red dots/lines) and probe light (blue dots/lines) on the Poincaré sphere under different initial pump SOP: (a) δ_+, (b) 45° linear polarization, elliptical polarization with ellipticity angles of (c) 3° and (d) 36°. The initial SOP of probe is set at δ_- in all cases.

According to Eqs. (5) and (7), the pump and probe light does not change over transmission since both the pump and probe are prepared in eigenstates. Actually, probe light launched in any polarization states does not change over transmission since the eigenvalues become degenerate in this case according to Eq. (7). Figure 1(b) shows the case of $|p| = |q|$, where the pump light is linearly polarized (LP). 45° LP is chosen in this case. It can be seen that the pump light does not evolve since that H_b' becomes proportional to an identity matrix, which is the reason why H_a' becomes z independent. The evolution of the probe light forms a single and closed circle on the Poincaré sphere, which is a general feature of z independent Hamiltonian. In the most general situations, i.e., $pq \neq 0$ and $|p| \neq |q|$, H_a' is z dependent and the eigenvectors and eigenvalues are found to be

$$\vec{u} = \left\{ \left\{ \frac{|p|\,|q|}{p^* q} e^{i\Delta\zeta_b z}, 1 \right\}, \left\{ -\frac{|p|\,|q|}{p^* q} e^{i\Delta\zeta_b z}, 1 \right\} \right\}, \quad \zeta_a = \frac{4}{3}\gamma P_p \left\{ 1 + |p|\,|q|, 1 - |p|\,|q| \right\}. \tag{8}$$

Figure 1(c) shows the case when the initial SOP of the pump light is elliptically polarized with a small ellipticity angle of 3°. In contrast to previous cases, pump light evolves along transmission which leads to the z dependence of the probe Hamiltonian. In this case, pump light traces a circle on the Poincaré sphere very close to the equator. Due to the z dependence of the probe Hamiltonian, probe light walks around the sphere by starting from the north pole, passing through a point which is very close to the south pole and back to the north pole again, as shown by the blue and purple lines. Only the first few cycles are plotted in Fig. 1(c) for clearance and the color is gradually tuned from blue to purple to indicate the evolution. The SOPs of the probe light cover almost the full Poincaré sphere except a small area encircled by the dotted line around the south pole. Figure 1(d) illustrates the case when the ellipticity angle of the pump light increases to 36°. Similarly, pump light traces a circle parallel but further away from the equator while the probe state walks around the sphere, covering less than half of the Poincaré sphere.

The rotation pattern of the pump and probe light can also be understood from the precession equations derived from the Hamiltonians, i.e., H_a' and H_b', following the procedure reported in [17], which is checked and consistent with that derived from MNLSE [5]. According to the precession equations, the SOP of the pump and probe light rotates around $\vec{m}_3$ and $\vec{m} - \vec{m}_3$, respectively, where $\vec{m}_3 = (\vec{m} \cdot \hat{k}_3)\hat{k}_3$. The fact that the evolution of the probe light could not cover the full Poincaré sphere in z dependent case is simply because the probe light rotates around an axis which evolves along propagation. We also emphasize that the advantage of adopting δ_+ and δ_- as mode basis is very clear from the Hamiltonian approach since δ_+ and δ_- are the eigenstates of the pump evolution

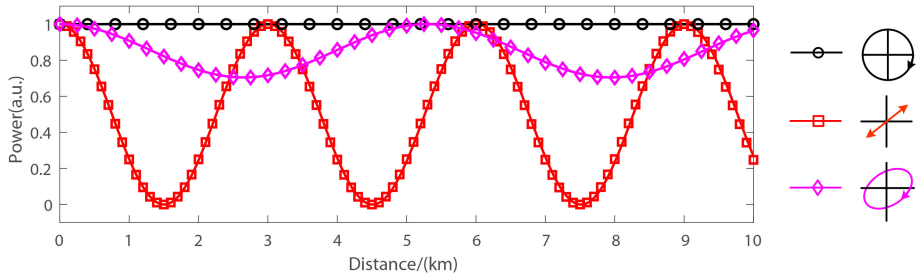

Fig. 2. Power distribution of the probe light in left-handed circularly polarized states (δ_-) for different initial pump states. Color black, red and magenta corresponds to δ_+, 45° linear polarization and elliptical polarization with ellipticity angles of 36°, respectively, as shown by the sketches with the corresponding color. The input pump/probe power is 28/0 dBm. Symbols and lines are calculated by Hamiltonian approach and nonlinear CMEs simulations, respectively. The numerical aperture of the simulated step-index multimode fiber is 0.205. The nonlinear coefficient of the fiber is $n_2 = 2.6 \times 10^{-20} m^2 W^{-1}$, and the effective area of the fundamental mode is $A_{eff} \approx 42.3$ um^2 corresponding to $\gamma \approx 2.49$ W^{-1}km^{-1}.

(Eq. (5)), providing a different angle from coupled mode equations where changing mode basis results in transforming the coherent coupling between x and y components into a linear coupling term [12].

To verify the proposed Hamiltonian approach, the power distribution of the probe light in δ_- over transmission distance is compared with direct numerical simulations of nonlinear coupled mode equations (CMEs), i.e., Eq. (1), as shown in Fig. 2. The parameters of the fiber used in simulations are given in the caption of Fig. 2. All curves start from 1 since the initial SOPs of the probe light are set at δ_- in all cases. The probe evolutions under different pump conditions shown in Fig. 1(a), 1(b) and 1(d) are plotted with black circles, red squares, magenta diamonds, respectively, corresponding to the situation where the probe light does not evolve, evolves with z independent Hamiltonian, and with z dependent Hamiltonian. The results calculated according to nonlinear CMEs are shown by the solid lines. It is clear that our method matches well with nonlinear CMEs simulations.

3.2 Scenario II: XMM Between Non-Degenerate Modes

Finally, we discuss scenario II, i.e., for sufficient large $\Delta\beta$. In practice, this corresponds to the non-degenerate mode case where the beat length L_B between two modes is much smaller than the nonlinear interaction length L_{NL}. As a result, the exponential factor in the H_a and H_b of Eq. (2) oscillates rapidly, contributing little to the pulse evolution process on average [12]. Neglecting these terms and defining the pump and probe as $|b\rangle = (b_1 \quad b_2)^T$ and $|a\rangle = (a_1 \quad a_2)^T$, respectively, with the initial condition of pump as $|b\rangle_{z=0} = \sqrt{P_p}(p \quad q)^T$, the Hamiltonian of the pump light and probe light are found to be

$$H_b'' = \gamma P_p \begin{pmatrix} s_1|p|^2 + s_2|q|^2 & 0 \\ 0 & s_3|p|^2 + s_4|q|^2 \end{pmatrix}, \tag{9a}$$

$$H_a'' = \gamma P_p \begin{pmatrix} s_5|p|^2 + s_6|q|^2 & s_7 pq^* e^{j\Delta\zeta_b z} \\ s_8 p^* q e^{-j\Delta\zeta_b z} & s_9|p|^2 + s_{10}|q|^2 \end{pmatrix}, \tag{9b}$$

where $s_1 = C_{3333}, s_2 = C_{3434} + C_{3443}, s_3 = C_{4343} + C_{4334}, s_4 = C_{4444}, s_5 = C_{1313} + C_{1331}, s_6 = C_{1414} + C_{1441}, s_7 = C_{1423} + C_{1432}, s_8 = C_{2314} + C_{2341}, s_9 = C_{2323} + C_{2332}, \quad s_{10} = C_{2424} + C_{2442}, \quad \Delta\zeta_b = \zeta_{b_1} - \zeta_{b_2}$ and ζ_b is given by H_b'' as

$$\zeta_b = \left\{\zeta_{b_1}, \zeta_{b_2}\right\} = \gamma P_p \left\{s_1|p|^2 + s_2|q|^2, s_3|p|^2 + s_4|q|^2\right\}. \tag{10}$$

In practice, $L_B \ll L_{NL}$ corresponds to the case where the XMM occurs between non-degenerate modes, especially those from different mode groups. As an example, the XMM effect between two

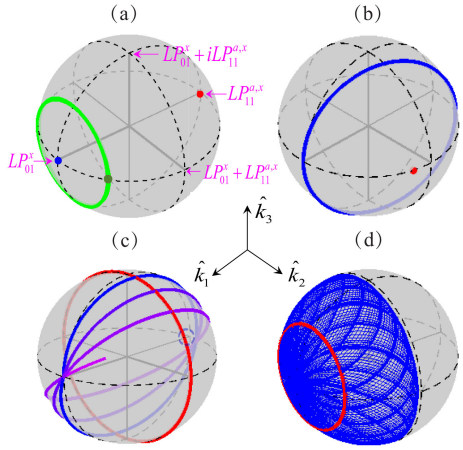

Fig. 3. Evolution of the modes of pump light (red dots/lines) and probe light (blue/green dots/lines) on the Bloch sphere under different initial pump light: (a) $p = 0, q = 1$, (b) $p = 0.79, q = 0.61$, (c) $p = q = \sqrt{2}/2$ and (d) $p = 2\sqrt{2}/3, q = 1/3$. $s_1 = 1, s_2 = s_3 = s_6 = s_7 = s_8 = s_9 = 1.18, s_4 = 0.88, s_5 = 2, s_{10} = 1.76$. The initial probe mode is set at LP_{01}^{x} in all cases except that the green line start from $2\sqrt{2}/3LP_{01}^{x} + 1/3LP_{11}^{a,x}$, as indicated by the dark green dot.

TABLE 1
Linearization of the XMM in Literatures and This Work

With RMM	Without RMM (This work)			
[1]		Scenario I: $L_B \gg L_{NL}$	Scenario II: $L_B \ll L_{NL}$	$L_B \sim L_{NL}$
[9]	$pq = 0$	Fig. 1(a)*	Fig. 3(a)*	Analytical Hamiltonian is not available
	$\lvert p\rvert = \lvert q\rvert$	Fig. 1(b)*	Fig. 3(c)$^+$	
	$pq \neq 0$, $\lvert p\rvert \neq \lvert q\rvert$	Fig. 1(c)$^+$, Fig. 1(d)$^+$	Fig. 3(b)*, Fig. 3(d)$^+$	

* Obtained numerically by Hamiltonian approach.
$^+$ Obtained analytically by Hamiltonian approach.

spatial modes that belongs to LP_{01} and LP_{11} mode group is studied. Fiber parameters are the same as in the case of $L_B \gg L_{NL}$. The polarization of the two modes are aligned at x polarization. Apart from polarization degeneracy, LP_{11} mode group has two-fold degeneracy with respect to spatial coordinates, one of which is chosen for the following analysis, named as LP_{11}^{a}. s_1 to s_{10} can thus be calculated according to the mode selected and are listed in the caption of Fig. 3. The evolution of pump and probe modes on the Bloch sphere are shown in Figure 3 with concrete definition of the axes illustrated in Fig. 3(a). Simiarly, Fig. 3(a)–(b)/Fig. 3(c)–(d) show the case where H_a'' is independent/dependent of z. In all cases, the initial probe state is set at LP_{01}^{x} except the green line shown in Fig 3(a) which will be discussed in a while. There are a few different features between scenario I and II. In the case of $pq = 0$ which is shown in Fig 3(a), the situation differs from $L_B \gg L_{NL}$ that the probe mode will change if not prepared in one of the eigenstates, due to the fact that the eigenvalues in this case is not degenerate, as shown by the green line. In case of $|p| = |q|$, $\zeta_{b_1} - \zeta_{b_2} \neq 0$ according to Eq. (10) under given s parameters. Therefore, the pump light evolves along propagation, as shown in Fig. 3(c). To satisfy $\zeta_{b_1} - \zeta_{b_2} = 0$, $p = 0.79$ and $q = 0.61$. This is the case shown in Fig. 3(b). The projection of the probe light on LP_{01}^{x} over transmission distance is checked and matched well with nonlinear CMEs simulations.

In the case of $L_B \sim L_{NL}$, analytical Hamiltonian is not available. The evolution of pump/probe light can be obtained by solving Eq. (2) numerically. The evolution of pump and probe states can thus be resolved sequentially over small steps using local states with nonlinear phase shifts. In this work, we propose a generalized Hamiltonian approach in the absence of RMM. It is shown that the Hamiltonian of the probe light is in general spatially dependent, which is fundamentally different from our previous analysis [9] where the Hamiltonian is independent of propagation coordinates.

As a consequence, the SOP of the probe light rotates around a fixed axis on the Poincaré sphere in the previous works with RMM [1], [9], similar to Fig. 1(a) and 1(b), Fig. 3(a) and 3(b). On the contrary, the SOP of the probe light on the Poincaré sphere can evolves in a more complicated fashion, i.e., around an axis that evolves with z, such as Fig. 1(c) and 1(d), Fig. 3(c) and 3(d).

4. Conclusion

As summarized in Table 1, we focus on the linearization of XMM effect in the absence of RMM, where nonlinear polarization rotation in single mode waveguides can be viewed as a special case. This work is relevant in a wide range of practical situations, such as XMM effect in optical fibers with high power ratings or in nanostructures featuring ultrashort interaction length etc. Two special scenarios regarding differential mode propagation constants are carefully discussed. By taking the advantage that the Hamiltonian of the pump light can be diagonalized in these two scenarios, the Hamiltonian of the probe light can be explicitly written out, which is in general spatial dependent and distinguished from the Hamiltonian derived in the presence of RMM. We emphasis that the Hamiltonian approach contributes a general but simple picture to understand the XMM nonlinear problem. For example, our approach highlights the eigenstates of the XMM system, leading to an intuitive explanation of selection of circularly polarized mode basis instead of LP mode basis. Although two mode situations are discussed for clearance, this work can be readily expanded to include more number of modes.

References

[1] D. I. Kroushkov, G. Rademacher, and K. Petermann, "Cross mode modulation in multimode fibers," *Opt. Lett.*, vol. 38, no. 10, pp. 1642–1644, May 2013.

[2] N. M. Lpken, T. Hellwig, M. Schnack, J. P. Epping, K. J. Boller, and C. Fallnich, "Low-power broadband all-optical switching via intermodal cross-phase modulation in integrated optical waveguides," *Opt. Lett.*, vol. 43, no. 8, pp. 1631–1634, Apr. 2018.

[3] Z. Pan, Y. Weng, and J. Wang, "Investigation of nonlinear effects in few-mode fibers," *Photon. Netw. Commun.*, vol. 31, no. 2, pp. 305–315, Apr. 2016.

[4] K. Kitayama, Y. Kimura, K. Okamoto, and S. Seikai, "Optical sampling using an allfiber optical kerr shutter," *Appl. Phys. Lett.*, vol. 46, no. 7, pp. 623–625, Apr. 1985.

[5] Q. Lin and G. P. Agrawal, "Vector theory of cross-phase modulation: Role of nonlinear polarization rotation," *IEEE J. Quantum Electron.*, vol. 40, no. 7, pp. 958–964, Jul. 2004.

[6] D. J. Richardson, J. M. Fini, and L. E. Nelson, "Space-division multiplexing in optical fibres," *Nature Photon.*, vol. 7, no. 5, pp. 354–362, May 2013.

[7] F. Poletti and P. Horak, "Description of ultrashort pulse propagation in multimode optical fibers," *J. Opt. Soc. Amer. B*, vol. 25, no. 10, pp. 1645–1654, Oct. 2008.

[8] J. Sakurai and J. Napolitano, *Modern Quantum Mechanics*, 2nd ed. London, U.K.: Pearson Harlow, 2014.

[9] H. Yang, W. Chen, H. Hu, J. Xu, Y. Chen, and X. Zhang, "On the Hamiltonian form of cross-mode modulation in nonlinear optical waveguides," *Opt. Lett.*, vol. 43, no. 20, pp. 5005–5008, Oct. 2018.

[10] X. Wu and L. Tong, "Optical microfibers and nanofibers," *Nanophotonics*, vol. 2, no. 5-6, pp. 407–428, Oct. 2013.

[11] A. Mecozzi, C. Antonelli, and M. Shtaif, "Nonlinear propagation in multi-mode fibers in the strong coupling regime," *Opt. Exp.*, vol. 20, no. 11, pp. 11 673–11 678, May 2012.

[12] G. P. Agrawal, *Nonlinear Fiber Optics*, 5th ed. New York, NY, USA: Academic, 2013.

[13] B. Daino, G. Gregori, and S. Wabnitz, "New all-optical devices based on third-order nonlinearity of birefringent fibers," *Opt. Lett.*, vol. 11, no. 1, pp. 42–44, Jan. 1986.

[14] C. Antonelli, M. Shtaif, and A. Mecozzi, "Modeling of nonlinear propagation in space-division multiplexed fiber-optic transmission," *J. Lightw. Technol.*, vol. 34, no. 1, pp. 36–54, Jan. 2016.

[15] S. Blanes, F. Casas, J. A. Oteo, and J. Ros, "A pedagogical approach to the magnus expansion," *Eur. J. Phys.*, vol. 31, no. 4, pp. 907–918, Jun. 2010.

[16] J. P. Gordon and H. Kogelnik, "PMD fundamentals: Polarization mode dispersion in optical fibers," *Proc. Nat. Acad. Sci.*, vol. 97, no. 9, pp. 4541–4550, Apr. 2000.

[17] L. Ranzani and J. Aumentado, "A geometric description of nonreciprocity in coupled two-mode systems," *New J. Phys.*, vol. 16, no. 10, Oct. 2014, Art. no. 103027.